A PDE-CONSTRAINED OPTIMIZATION FORMULATION FOR DISCRETE FRACTURE NETWORK FLOWS[*]

STEFANO BERRONE[†], SANDRA PIERACCINI[†], AND STEFANO SCIALÒ[†]

Abstract. We investigate a new numerical approach for the computation of the three-dimensional flow in a discrete fracture network that does not require a conforming discretization of partial differential equations on complex three-dimensional systems of planar fractures. The discretization within each fracture is performed independently of the discretization of the other fractures and of their intersections. An independent meshing process within each fracture is a very important issue for practical large-scale simulations, making mesh generation easier. Some numerical simulations are given to show the viability of the method. The resulting approach can be naturally parallelized for dealing with systems with a huge number of fractures.

Key words. fracture flows, Darcy flows, discrete fracture networks, optimization methods for elliptic problems, uncoupled large scale simulations

AMS subject classifications. 65N30, 65N15, 65N50, 65J15

DOI. 10.1137/120865884

1. Introduction. Efficient numerical simulations of subsurface fluid flows in fractured rocks are of interest for many applications, including water resources management, contaminant transport and dissemination, oil prospecting, and enhanced oil/gas recovery. Among the major difficulties are intrinsic heterogeneity, directionality of the medium, and the multiscale nature of the phenomena, as well as uncertainty in the medium properties. A discrete fracture network (DFN) is a complex three-demensional (3D) structure obtained from intersecting planar fractures. DFN models are frequently preferred to more conventional continuum models as a basis for simulations. A classical approach to the problem is to model fractures as planar ellipses or polygons and stochastically generate DFNs with probabilistic distributions of density, aspect ratio, orientation, size, aperture of fractures, and hydrologic properties [9] and to simulate the flow through the obtained networks. Intensive numerical simulations with several configurations of DFNs and physical parameters are then performed in order to tackle the issue of uncertainty. The flow pattern strongly depends on density and size of fractures and for large-scale simulations different approaches are possible. For dense fracture networks and continuous distribution of size and aspect ratios, flow can be modeled as the flow in an equivalent continuous porous medium where the fracture network pattern leads to the definition of a suitable permeability tensor. For sparse fracture networks with some large fractures that discontinuously increase directionality of the flow, an explicit representation of the fracture network is more reliable. In both cases a stochastic approach to the uncertainty of the parameters is needed and this requires many simulations, so that efficiency and large applicability of numerical algorithms are fundamental issues.

[†]Dipartimento di Scienze Matematiche, Politecnico di Torino, Corso Duca degli Abruzzi 24, 10129 Torino, Italy (stefano.berrone@polito.it, sandra.pieraccini@polito.it, stefano.scialo@polito.it).

Here the steady flow in a given DFN is considered under the assumption of impervious rock matrix and no longitudinal flow in the intersection between the fractures. These intersections are called *traces* and are always segments.

In DFN simulations the first classical numerical challenge is to provide a good-quality conforming mesh for this 3D structure to be used for the discretization of the flow equations. Conformity of the mesh requires that for each trace a unique discretization is introduced, which is shared by all the discretizations of the fractures intersecting along the trace. Conformity on the traces and good quality of the meshes for a completely arbitrary DFN can be obtained only with the introduction of a huge number of elements independently of the required accuracy of the numerical solution. In [28], a mixed nonconforming finite element method (FEM) on a conforming mesh is proposed. In [20], an adaptive approach to the conforming mesh generation requiring adjustments of trace spatial collocations is proposed. Local modifications of the mesh or of the fracture network in order to preserve conformity of the meshes or alignment of meshes along the traces are considered in several works as for example [17, 28]. In [11], a method to generate a good-quality conforming mesh on the network system is proposed. In [23, 24], a mixed hybrid mortar method is proposed, allowing nonconformities of the meshes on the fractures but requiring that the traces are contained in the set of the edges of each fracture triangulation. Resorting to mortar methods the discretization of each fracture can lead to a different discretization of the traces. A different approach to the simulation of the flow in the fracture network is based on its modelization with a system of monodimensional pipes that are aligned along the fractures and mutually connect the centers of the fracture intersections with the surrounding fractures. The resulting mesh of pipes still reflects the topological properties of the fracture network [6, 22]. An accurate definition of pipe properties within the fracture system has been obtained by means of a boundary element method in [10]. However, the geometrical simplification implies errors in the assessment of the fluid flow regime, depending on the complexity and geometrical properties of the underlying DFN, and thus the resort to a full discretization is preferred.

Specific commercial codes based on the FEM are available, also simulating the fluid flow in the rock blocks [19]; contributions can be found in the literature for the extension to coupled problems with deformable blocks and fractures, even in conjunction with other methods such as the boundary element mothod (e.g., [12]). However, these codes suffer for a strong computational demand: the discretization in fact leads frequently to the generation of huge or poor-quality meshes.

The problem model allows discontinuities of fluxes of the hydraulic head through the traces when fluxes of the hydraulic head leave a fracture to reach a different fracture at the common trace. With previous approaches these discontinuities can be modeled if they are localized at edges between elements or at the border of each piece of fracture.

In this paper a new method is proposed, which relies on the reformulation of the problem as a PDE-constrained optimization problem. Following this approach, fracture meshes are not required to match along traces and any kind of mesh conformity along traces is skipped, thus making the mesh generation process an easy task, attainable with a standard mesh generator. Furthermore, the problem on the overall DFN can be decoupled in several local problems on the fractures, thus allowing a great potential for possible parallel implementation. Discontinuities of fluxes of the hydraulic head can occur on arbitrary traces with respect to the triangulation and the used finite elements allow us to catch these discontinuities of the fluxes also inside elements. This can be obtained by introducing suitable extended finite elements.

The paper is organized as follows. In section 2, we recall the physical model and governing equations and introduce the continuous optimization problem that leads to the solution on the network system. In section 3 we recall basics on extended finite elements of the type considered herein and give some details for the application to DFNs. In section 4 a discrete formulation of the optimization problem is given, which leads to an equality constrained quadratic programming problem. Finally, in section 5 numerical results are discussed in order to prove the viability, reliability, and effectiveness of the method.

Notation. In the paper, we will frequently use the following notation. We will use capital letters for continuous unknowns (for example, the hydraulic head H) and lowercase letters for the corresponding finite dimensional approximation (e.g., h). We will use the same lowercase letter for the vector of degrees of freedom (DOFs), the difference being clear from the context. Roman capital letters will be used for functional spaces. Given functions g_i, for i belonging to some index set I, the symbol $\prod_{i \in I} g_i$ denotes the tuple of functions $(g_1, g_2, \ldots, g_{\#I})$, $\#I$ being the cardinality of I.

2. Description of the problem.

2.1. The continuous problem. Let us consider an open planar polygonal fracture $\omega \subset \mathbb{R}^2$ and let us introduce on ω a tangential coordinate system $\hat{x}$. Following [1], the problem of subsurface flow through ω can be written as

$$-\nabla \cdot (\mathbf{K} \nabla H) = q \qquad \text{in } \omega, \tag{2.1}$$

$$H_{|_{\Gamma_D}} = H_D \qquad \text{on } \gamma_D, \tag{2.2}$$

$$\frac{\partial H}{\partial \hat{\nu}} = G_N \qquad \text{on } \gamma_N, \tag{2.3}$$

where $\partial \omega = \gamma_D \cup \gamma_N$ is the boundary of ω and $\gamma_D \cap \gamma_N = \emptyset$, $\gamma_D \neq \emptyset$. The scalar function $H = \mathcal{P} + \zeta$ is the hydraulic head, $\mathcal{P} = p/(\varrho g)$ is the pressure head, p is the fluid pressure, g is the gravitational acceleration, and ϱ is the fluid density. The variable ζ is the elevation, and $\mathbf{K} = \mathbf{K}(\hat{x})$ is the fracture transmissivity tensor and is a symmetric and uniformly positive definite tensor. The symbol $\frac{\partial H}{\partial \hat{\nu}}$ denotes the outward co-normal derivative of the hydraulic head,

$$\frac{\partial H}{\partial \hat{\nu}} = \hat{n}^T \mathbf{K} \nabla H,$$

with $\hat{n}$ unit vector outward normal to the boundary γ_N.

The definition of the hydraulic head in a DFN Ω should require the solution of problem (2.1)–(2.3) in a system of intersected polygonal fractures in the space. In order to define 3D fractures F_i, let us consider a set of open planar polygons $\{\omega_i\}_{i \in \mathfrak{I}}$, where $\mathfrak{I}$ is the set of their indices, and let $\bar{F}_i \subset \mathbb{R}^3$ be the image of the closure of a polygon $\omega_i \subset \mathbb{R}^2$ through an affine mapping $T_i(\hat{x}_i) = b_i + Q_i(\hat{x}_i - \hat{x}_{0,i})$, where $\hat{x}_{0,i}$ is the coordinate of a given vertex of the polygon ω_i in the local planar reference system $\hat{x}_i$, and b_i is the position of the same vertex in the 3D space. We assume that $Q_i^T Q_i$ is the identity matrix such that the differential operators defined on the tangential reference system in F_i are equivalent to the operators defined on the planar fracture ω_i. Let Ω be the 3D set

$$\Omega = \bigcup_{i \in \mathfrak{I}} F_i,$$

and let $\partial \Omega$ denote its boundary. Given two fractures, the intersection of their closure is either an empty set or a set of nonvanishing segments called *traces*. Vanishing
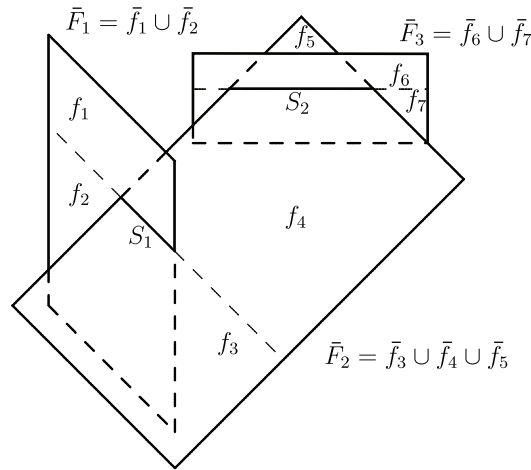
FIG. 2.1. *An example of DFN split into subfractures.*

segments are not considered as no flux exchange among fractures takes place in these intersections. Let $\mathcal{S}$ denote the set of all the traces, and assume traces in $\mathcal{S}$ are indexed by a set of indices $\mathfrak{M}$ with cardinality $\sharp\mathfrak{M}$.

In what follows, we make the following assumptions on the DFN:

1. $\bar{\Omega}$ is a connected set;
2. each trace S_m, $m \in \mathfrak{M}$, is shared by exactly two polygonal fractures F_i and F_j, $i \neq j$: $S_m \subseteq \bar{F}_i \cap \bar{F}_j$;
3. on each fracture, the transmissivity tensor $\mathbf{K}_i(\hat{x}_i)$ is symmetric and uniformly positive definite.

Given a trace S_m we denote by $I_{S_m} = \{i, j\}$ the set of indices i and j of the fractures F_i and F_j sharing the trace; for further convenience, we also introduce the sorted couple $c_m = (i, j)$ with $i < j$. For each fracture F_i, we denote by $\mathcal{S}_i$ the set of traces shared by F_i and other fractures.

In order to define the problem on the DFN, let us consider a set of open subfractures f_l, $l \in \mathfrak{L}$, obtained by splitting each fracture in such a way that each trace is part of the boundary of some subfractures and $S_m \cap f_l = \emptyset$ $\forall m \in \mathfrak{M}, \forall l \in \mathfrak{L}$; see Figure 2.1. Note that the traces belong to the boundary of the subfractures, but they do not necessarily coincide with a whole edge of such boundaries; see, e.g., trace S_2 in Figure 2.1. So we have

$$\Omega = \bigcup_{l \in \mathfrak{L}} \bar{f}_l \backslash \partial\Omega.$$

Let us split $\partial\Omega$ in two parts $\Gamma_D \neq \emptyset$ and Γ_N, with $\partial\Omega = \Gamma_D \cup \Gamma_N$ and $\Gamma_D \cap \Gamma_N = \emptyset$, corresponding to Dirichlet and Neumann boundary conditions, respectively.

The global hydraulic head H in the whole connected system Ω satisfies the following equations $\forall l \in \mathfrak{L}$:

$$(2.4) \qquad \nabla \cdot (\mathbf{K}_{f_l} \nabla H) = q_l \qquad \text{in } f_l,$$

$$(2.5) \qquad H_{|_{\Gamma_D \cap \partial f_l}} = H_D \qquad \text{on } \Gamma_D \cap \partial f_l,$$

$$(2.6) \qquad \frac{\partial H}{\partial \hat{\nu}_{\partial f_l}} = G_N \qquad \text{on } \Gamma_N \cap \partial f_l,$$

with a two-dimensional (2D) local reference system on f_l. Given a trace S_m let $\mathfrak{L}_{S_m} \subset \mathfrak{L}$ be the set of indices l such that $S_m \subset \partial f_l$. Equations (2.4)–(2.6) have to be complemented with the following coupling conditions, corresponding to the physical requirement of continuity of the hydraulic head and conservation of hydraulic fluxes across the traces:

$$(2.7) \qquad H_{|_{\bar{f}_l}} = H_{|_{\bar{f}_k}} \text{ on } S_m \qquad \forall S_m \in \mathcal{S}, \ \forall l, k \in \mathfrak{L}_{S_m},$$

$$(2.8) \qquad \sum_{l \in \mathfrak{L}_{S_m}} \frac{\partial H_{|_{f_l}}}{\partial \hat{\nu}_{\partial f_l}} = 0 \quad \text{ on } S_m \qquad \forall S_m \in \mathcal{S}.$$

For this formulation of the problem existence and uniqueness of the solution are known. In the following we want to focus on the whole fracture, disregarding this subfracture approach. Thus, let us denote by H_i the restriction of the hydraulic head H to the fracture F_i $\forall i \in \mathfrak{I}$. Conditions (2.7) and (2.8) are equivalent to

$$(2.9) \qquad H_{i|S_m} - H_{j|S_m} = 0 \qquad \text{for } i, j \in I_{S_m} \ \forall m \in \mathfrak{M},$$

$$(2.10) \qquad \left[\!\!\left[\frac{\partial H_i}{\partial \hat{\nu}_{S_m}^i} \right]\!\!\right]_{S_m} + \left[\!\!\left[\frac{\partial H_j}{\partial \hat{\nu}_{S_m}^j} \right]\!\!\right]_{S_m} = 0 \qquad \text{for } i, j \in I_{S_m},$$

where the symbol $\left[\!\!\left[\frac{\partial H_i}{\partial \hat{\nu}_{S_m}^i} \right]\!\!\right]$ denotes the jump of the co-normal derivative along the unique normal $\hat{n}_{S_m}^i$ fixed for the trace S_m on the fracture F_i. This jump is independent of the orientation of $\hat{n}_{S_m}^i$.

Let Γ_i be the boundary of F_i and let it be split in Γ_{iN}, the boundary with Neumann boundary condition $\frac{\partial H_i}{\partial \nu} = G_{iN}$, and $\Gamma_{iD} \neq \emptyset$, the boundary with Dirichlet boundary condition $H_{i|_{\Gamma_D}} = H_{iD}$, satisfying $\Gamma_{iN} \cap \Gamma_{iD} = \emptyset$ and $\Gamma_{iN} \cup \Gamma_{iD} = \Gamma_i$. Let us define

$$V_i = \mathrm{H}_0^1(F_i) = \left\{ v \in \mathrm{H}^1(F_i) : v_{|_{\Gamma_{iD}}} = 0 \right\}$$

and V_i' its dual space. The hydraulic head H_i in each fracture belongs to the space

$$V_i^D = \mathrm{H}_{\mathrm{D}}^1(F_i) = \left\{ v \in \mathrm{H}^1(F_i) : v_{|_{\Gamma_{iD}}} = H_{iD} \right\}$$

and the hydraulic head H on the whole domain Ω is obtained by suitably matching via (2.9), (2.10) for $m \in \mathfrak{M}$ the solutions $H_i \in V_i^D$ for each $i \in \mathfrak{I}$ and belongs to the space

$$(2.11) \quad V^D = \mathrm{H}_{\mathrm{D}}^1(\Omega) = \left\{ v \in \prod_{i \in \mathfrak{I}} V_i^D : (v_{|_{F_i}})_{|_{S_m}} = (v_{|_{F_j}})_{|_{S_m}}, \ i, j \in I_{S_m}, \ \forall m \in \mathfrak{M} \right\}.$$

With a similar definition we set $V = \mathrm{H}_0^1(\Omega)$.

For simplicity of notation, in the rest of this section we assume that the traces $S \in \mathcal{S}$ are disjoint.

Remark 2.1. The assumption of disjoint traces can be removed by replacing, in what follows, each single trace S with the union of connected traces. Furthermore, in our discrete formulation, this assumption is dropped out in a natural way; see Remark 4.1.

Let us define for each trace $S \in \mathcal{S}$ a suitable space $\mathcal{U}^S$ and

$$\mathcal{U}^{\mathcal{S}_i} = \prod_{S \in \mathcal{S}_i} \mathcal{U}^S, \qquad \mathcal{U} = \prod_{i \in \mathfrak{I}} \mathcal{U}^{\mathcal{S}_i}.$$

Moreover, for each trace $S \in \mathcal{S}$, with $I_S = \{i, j\}$, we introduce suitable variables $U_i^S \in \mathcal{U}^S$ and $U_j^S \in \mathcal{U}^S$ representing the unknown quantities $\left[\!\left[\frac{\partial H_i}{\partial \hat{\nu}_S^i} \right]\!\right]$ and $\left[\!\left[\frac{\partial H_j}{\partial \hat{\nu}_S^j} \right]\!\right]$, respectively, and for each fracture F_i let us set

$$U_i = \prod_{S \in \mathcal{S}_i} U_i^S \in \mathcal{U}^{\mathcal{S}_i},$$

i.e., U_i is the tuple of functions U_i^S with S spanning $\mathcal{S}_i$. Moreover, we set

$$U = \prod_{i \in \mathfrak{I}} U_i \in \mathcal{U}$$

as the tuple of all functions U_i^S with $S \in \mathcal{S}_i$ and $i \in \mathfrak{I}$, i.e., U is the $2\#\mathfrak{M}$-tuple of functions U_i^S on all traces in Ω.

Condition (2.10) is rewritten, in terms of the new unknowns $U_i^{S_m}$, $U_j^{S_m}$, as

$$(2.12) \qquad\qquad U_i^{S_m} + U_j^{S_m} = 0 \qquad \text{for } i, j \in I_{S_m}.$$

Let us introduce the linear bounded operators and their duals

$$A_i \in \mathcal{L}(V_i, V_i'), \qquad A_i^* \in \mathcal{L}(V_i, V_i'), \qquad A_i^D \in \mathcal{L}(V_i^D, V_i'),$$
$$B_i \in \mathcal{L}(\mathcal{U}^{\mathcal{S}_i}, V_i'), \qquad B_i^* \in \mathcal{L}(V_i, \mathcal{U}^{\mathcal{S}_i\prime}), \qquad B_{\Gamma_{iN}} \in \mathcal{L}(\mathrm{H}^{-\frac{1}{2}}(\Gamma_{iN}), V_i'),$$

and the Riesz isomorphism $\Lambda_{\mathcal{U}^{\mathcal{S}_i}} : \mathcal{U}^{\mathcal{S}_i} \to \mathcal{U}^{\mathcal{S}_i\prime}$. The operators A_i, A_i^D, B_i, $B_{\Gamma_{iN}}$ are defined such that

$$\langle A_i H_i^0, v \rangle_{V_i', V_i} = \left(\mathbf{K} \nabla H_i^0, \nabla v \right), \ H_i^0 \in V_i, \ v \in V_i,$$
$$\langle A_i^D H_i^D, v \rangle_{V_i', V_i} = (\mathbf{K} \nabla H_i^D, \nabla v), \ H_i^D \in V_i^D, \ v \in V_i,$$
$$\langle B_i U_i, v \rangle_{V_i', V_i} = \langle U_i, v_{|_{\mathcal{S}_i}} \rangle_{\mathcal{U}^{\mathcal{S}_i}, \mathcal{U}^{\mathcal{S}_i\prime}}, \ U_i \in \mathcal{U}^{\mathcal{S}_i}, v \in V_i,$$
$$\langle B_{\Gamma_{iN}} G_{iN}, v \rangle_{V_i', V_i} = \langle G_{iN}, v_{|_{\Gamma_{iN}}} \rangle_{\mathrm{H}^{-\frac{1}{2}}(\Gamma_{iN}), \mathrm{H}^{\frac{1}{2}}(\Gamma_{iN})}, \ G_{iN} \in \mathrm{H}^{-\frac{1}{2}}(\Gamma_{iN}), v \in V_i.$$

Finally, let $\mathcal{R}_i H_{iD} \in V_i^D$ be a lifting of Dirichlet boundary condition H_{iD}.

Let us introduce $\forall i \in \mathfrak{I}$ the following problem: find $H_i = H_i^0 + \mathcal{R}_i H_{iD}$ with $H_i^0 \in V_i$ such that

$$\left(\mathbf{K} \nabla H_i^0, \nabla v \right) = (q_i, v) + \langle U_i, v_{|_{\mathcal{S}_i}} \rangle_{\mathcal{U}^{\mathcal{S}_i}, \mathcal{U}^{\mathcal{S}_i\prime}}$$
$$(2.13) \qquad\qquad + \langle G_{iN}, v_{|_{\Gamma_{iN}}} \rangle_{\mathrm{H}^{-\frac{1}{2}}(\Gamma_{iN}), \mathrm{H}^{\frac{1}{2}}(\Gamma_{iN})} - (\mathbf{K} \nabla \mathcal{R}_i H_{iD}, \nabla v) \quad \forall v \in V_i$$

or equivalently $\forall i \in \mathfrak{I}$

$$(2.14) \qquad\qquad A_i H_i^0 = q_i + B_i U_i + B_{iN} G_{iN} - A_i^D \mathcal{R}_i H_{iD}.$$

The following result states the equivalence between the subfracture setting and the setting based on fractures. The proof is omitted as it straightforwardly follows from classical arguments.

PROPOSITION 2.2. *Let $\mathcal{U}^S = \mathrm{H}^{-\frac{1}{2}}(S) \forall S \in \mathcal{S}$. Then, solving (2.13) $\forall i \in \mathfrak{I}$ with additional conditions (2.9), (2.12) is equivalent to solving (2.4)–(2.8).*

2.2. The optimal control formulation. The formulation of the problem described in the previous section requires the exact fullfilment of some conditions which couple the solution on different fractures; this happens either in the subfracture setting given by (2.4)–(2.8) or with the formulation (2.13) with coupling conditions (2.9), (2.12). Hence, finding a numerical solution to the problem solving the previous sets of equations typically asks for some form of (at least partial) conformity in the meshes introduced on the fractures; see, e.g., [11, 17, 20, 23, 28].

In order to circumvent this problem, we propose here a different approach. Instead of solving the coupled differential problems, we look for the solution of a PDE-constrained optimal control problem [18], the variable U being the "control variable." Let us define for each trace $S \in \mathcal{S}$ a suitable space $\mathcal{H}^S$, the spaces

$$\mathcal{H}^{\mathcal{S}_i} = \prod_{S \in \mathcal{S}_i} \mathcal{H}^S, \qquad \mathcal{H} = \prod_{i \in \mathfrak{I}} \mathcal{H}^{\mathcal{S}_i},$$

and the Riesz isomorphism $\Lambda_{\mathcal{H}^{\mathcal{S}_i}} : \mathcal{H}^{\mathcal{S}_i} \to \mathcal{H}^{\mathcal{S}_i}{}'$. The linear bounded "observation" operators C_i^S and C_i and the dual C_i^*

$$C_i^S \in \mathcal{L}(V_i, \mathcal{H}^S), \qquad C_i \in \mathcal{L}(V_i, \mathcal{H}^{\mathcal{S}_i}) = \prod_{S \in \mathcal{S}_i} C_i^S, \qquad C_i^* \in \mathcal{L}(\mathcal{H}^{\mathcal{S}_i}{}', V_i')$$

will be defined for each choice of the spaces $\mathcal{H}^S$. For all $i \in \mathfrak{I}$, let us denote by $H_i(U_i)$ the solution to (2.13) corresponding to the value U_i for the control variable. Furthermore, fixing a fracture F_i, we denote by

$$\prod_{S \in \mathcal{S}_i} U_j^S$$

the tuple of control variables defined on fractures F_j intersecting F_i in traces $S \in \mathcal{S}_i$ and by

$$\prod_{S \in \mathcal{S}_i} \left(C_i^S H_i(U_i) - C_j^S H_j(U_j) \right)$$

the tuple of functions $\left(C_i^S H_i(U_i) - C_j^S H_j(U_j) \right)$ as S varies in $\mathcal{S}_i$.

Let us now introduce the following differentiable functional $J : \mathcal{U} \to \mathbb{R}$:

$$
\begin{aligned}
J(U) &= \sum_{S \in \mathcal{S}} J^S(U) = \sum_{S \in \mathcal{S}} \left(\|C_i^S H_i(U_i) - C_j^S H_j(U_j)\|_{\mathcal{H}^S}^2 + \|U_i^S + U_j^S\|_{\mathcal{U}^S}^2 \right) \\
&= \frac{1}{2} \sum_{i \in \mathfrak{I}} \sum_{S \in \mathcal{S}_i} \left(\|C_i^S H_i(U_i) - C_j^S H_j(U_j)\|_{\mathcal{H}^S}^2 + \|U_i^S + U_j^S\|_{\mathcal{U}^S}^2 \right)
\end{aligned}
$$

$$(2.15) \qquad = \frac{1}{2} \sum_{i \in \mathfrak{I}} \left(\| \prod_{S \in \mathcal{S}_i} \left(C_i^S H_i(U_i) - C_j^S H_j(U_j) \right) \|_{\mathcal{H}^{\mathcal{S}_i}}^2 + \|U_i + \prod_{S \in \mathcal{S}_i} U_j^S\|_{\mathcal{U}^{\mathcal{S}_i}}^2 \right).$$

PROPOSITION 2.3. *Let us define the spaces $\mathcal{U}^S$ and $\mathcal{H}^S$ and the observation operator C_i^S on the trace S as*

$$(2.16) \qquad \mathcal{U}^S = \mathrm{H}^{-\frac{1}{2}}(S), \qquad \mathcal{H}^S = \mathrm{H}^{\frac{1}{2}}(S), \qquad C_i^S H_i = H_{i|S} \ \forall S \in \mathcal{S}.$$

Then, the hydraulic head $H \in \mathrm{H}_{\mathrm{D}}^1(\Omega)$ is the unique exact solution of (2.4)–(2.8) if and only if it satisfies the differential problems (2.13) $\forall i \in \mathfrak{I}$ and, correspondingly, $J(U) = 0$.

Proof. The existence and uniqueness of $H \in \mathrm{H}^1_\mathrm{D}(\Omega)$ satisfying (2.4)–(2.8) is a classical result (see, for example, [28] and references therein). Proposition 2.2 states that problems (2.4)–(2.8) $\forall l$ are equivalent to problems (2.13) $\forall i$, endowed with matching conditions (2.9)–(2.12), which in turn are equivalent to $J(U) = 0$. $\quad\square$

Based on the previous proposition, the problem of finding the hydraulic head in the whole domain is restated here as follows: find $U \in \mathcal{U}$ solving the problem

$$(2.17) \qquad\qquad \min J(U) \quad \text{subject to (2.13)} \ \forall i \in \mathfrak{I}.$$

PROPOSITION 2.4. *The optimal control $U \in \mathcal{U}$ providing the solution to* (2.17) *corresponds to*

$$(2.18) \qquad (\Lambda_{\mathcal{U}^{s_i}})^{-1} B_i^* P_i + U_i + \prod_{S \in \mathcal{S}_i} U_j^S = 0 \qquad \forall i \in \mathfrak{I},$$

where the functions $P_i \in V_i \ \forall i \in \mathfrak{I}$ are the solutions to the equations

$$(2.19) \qquad A_i^* P_i = C_i^* \Lambda_{\mathcal{H}^{s_i}} \prod_{S \in \mathcal{S}_i} \left(C_i^S H_i - C_j^S H_j \right).$$

Proof. Let us differentiate the cost functional $J(U)$ with respect to the control U_i; this has effect only for $S \in \mathcal{S}_i$ and we have

$$
\begin{aligned}
J'(U)(v_i - U_i) &= \sum_{S \in \mathcal{S}_i} J^{S'}(U_i)(v_i - U_i) \\
&= \sum_{S \in \mathcal{S}_i} \Big[2 \left(C_i^S H_i(U_i) - C_j^S H_j(U_j), C_i^S (H_i(v_i) \right. \\
&\quad - H_i(U_i)))_{\mathcal{H}^S} + 2 \left(U_i^S + U_j^S, v_i^S - U_i^S \right)_{\mathcal{U}^S} \Big] \\
&= 2 \left\langle C_i^* \Lambda_{\mathcal{H}^{s_i}} \prod_{S \in \mathcal{S}_i} (C_i^S H_i(U_i) - C_j^S H_j(U_j)), H_i(v_i) - H_i(U_i) \right\rangle_{V_i', V_i} \\
&\quad + 2 \left\langle \Lambda_{\mathcal{U}^{s_i}} (U_i + \prod_{S \in \mathcal{S}_i} U_j^S), v_i - U_i \right\rangle_{\mathcal{U}^{s_i'}, \mathcal{U}^{s_i}} \\
&= 2 \left\langle A_i^* P_i, A_i^{-1} B_i (v_i - U_i) \right\rangle_{V_i', V_i} \\
&\quad + 2 \left\langle \Lambda_{\mathcal{U}^{s_i}} (U_i + \prod_{S \in \mathcal{S}_i} U_j^S), v_i - U_i \right\rangle_{\mathcal{U}^{s_i'}, \mathcal{U}^{s_i}} \\
&= 2 \left\langle B_i^* P_i, v_i - U_i \right\rangle_{\mathcal{U}^{s_i'}, \mathcal{U}^{s_i}} \\
&\quad + 2 \left\langle \Lambda_{\mathcal{U}^{s_i}} (U_i + \prod_{S \in \mathcal{S}_i} U_j^S), v_i - U_i \right\rangle_{\mathcal{U}^{s_i'}, \mathcal{U}^{s_i}}
\end{aligned}
$$

and this yields the thesis. $\quad\square$

Equations (2.13), (2.18), and (2.19) $\forall i \in \mathfrak{I}$ then provide a solution to the subsurface flow in the network; nevertheless, they couple all the unknowns on the overall DFN. As an alternative approach, we propose to set up a minimization process that only requires, at each step, local solutions on the fractures. The key point of this approach is that the method only requires *decoupled* solutions of the flows on fractures, thus avoiding mesh conformity requirements. This target is attained, for example, by using a gradient-based approach, such as the steepest descent method. This approach requires the solution of many simple problems with a small exchange of data. The resulting algorithm is suitable for massively parallel computers and GPU-based computers.

In order to describe the minimization process leading to the solution of the continuous problem (2.17), let us define

$$(2.20) \qquad \delta U_i = \Lambda_{\mathcal{U}^{S_i}}^{-1} B_i^* P_i + U_i + \prod_{S \in \mathcal{S}_i} U_j^S \ \forall i \in \mathfrak{I}, \qquad \delta U = \prod_{i \in \mathfrak{I}} \delta U_i,$$

and let $\delta H_i \in V_i \ \forall i \in \mathfrak{I}$ be defined as the solution of the problem

$$(2.21) \qquad\qquad\qquad A_i \delta H_i = B_i \delta U_i.$$

PROPOSITION 2.5. *Given a control variable U, let us increment it by a step $\lambda \delta U$. The steepest descent method corresponds to the stepsize*

$$(2.22) \qquad \lambda = -\frac{||\delta U||_{\mathcal{U}}^2}{\sum_{S \in \mathcal{S}} \left(||C_i^S \delta H_i - C_j^S \delta H_j||_{\mathcal{H}^S}^2 + ||\delta U_i^S + \delta U_j^S||_{\mathcal{U}^S}^2\right)},$$

where $\delta U_i^S = \delta U_{i|_S}$.

Proof. Let us compute $J(U + \lambda \delta U)$. We have

$$J(U + \lambda \delta U) = J(U) + 2 \sum_{S \in \mathcal{S}} \left(C_i^S H_i(U_i) - C_j^S H_j(U_j), \lambda(C_i^S \delta H_i - C_j^S \delta H_j)\right)_{\mathcal{H}^S}$$

$$+ 2 \sum_{S \in \mathcal{S}} \left(U_i^S + U_j^S, \lambda(\delta U_i^S + \delta U_j^S)\right)_{\mathcal{U}^S} + \lambda^2 \sum_{S \in \mathcal{S}} ||C_i^S \delta H_i - C_j^S \delta H_j||_{\mathcal{H}^S}^2$$

$$+ \lambda^2 ||\delta U_i^S + \delta U_j^S||_{\mathcal{U}^S}^2$$

$$= J(U) + 2 \sum_{i \in \mathfrak{I}} \sum_{S \in \mathcal{S}_i} \left(C_i^S H_i(U_i) - C_j^S H_j(U_j), \lambda C_i^S \delta H_i\right)_{\mathcal{H}^S}$$

$$+ 2 \sum_{i \in \mathfrak{I}} \sum_{S \in \mathcal{S}_i} \left(U_i^S + U_j^S, \lambda \delta U_i^S\right)_{\mathcal{U}^S}$$

$$+ \lambda^2 \sum_{S \in \mathcal{S}} \left(||C_i^S \delta H_i - C_j^S \delta H_j||_{\mathcal{H}^S}^2 + ||\delta U_i^S + \delta U_j^S||_{\mathcal{U}^S}^2\right)$$

$$= J(U) + 2 \sum_{i \in \mathfrak{I}} \left(\prod_{S \in \mathcal{S}_i} (C_i^S H_i(U_i) - C_j^S H_j(U_j)), \lambda C_i \delta H_i\right)_{\mathcal{H}^{S_i}}$$

$$+ 2 \sum_{i \in \mathfrak{I}} \left(U_i + \prod_{S \in \mathcal{S}_i} U_j^S, \lambda \delta U_i\right)_{\mathcal{U}^{S_i}}$$

$$+ \lambda^2 \sum_{S \in \mathcal{S}} \left(||C_i^S \delta H_i - C_j^S \delta H_j||_{\mathcal{H}^S}^2 + ||\delta U_i^S + \delta U_j^S||_{\mathcal{U}^S}^2\right).$$

From the previous relation, recalling (2.19) we obtain

$$J(U + \lambda \delta U) - J(U) - \lambda^2 \sum_{S \in \mathcal{S}} (||C_i^S \delta H_i - C_j^S \delta H_j||_{\mathcal{H}^S}^2 + ||\delta U_i^S + \delta U_j^S||_{\mathcal{U}^S}^2)$$

$$= 2\lambda \sum_{i \in \mathfrak{I}} \left\langle A_i^* P_i, A_i^{-1} B_i \delta U_i \right\rangle_{V_i', V_i} + 2\lambda \sum_{i \in \mathfrak{I}} \left\langle \Lambda_{\mathcal{U}^S}(U_i + \prod_{S \in \mathcal{S}_i} U_j^S), \delta U_i \right\rangle_{\mathcal{U}^{S_i'}, \mathcal{U}^{S_i}}$$

$$= 2\lambda \sum_{i \in \mathfrak{I}} \left\langle \Lambda_{\mathcal{U}^{S_i}}^{-1} B_i^* P_i + U_i + \prod_{S \in \mathcal{S}_i} U_j^S, \delta U_i \right\rangle_{\mathcal{U}^{S_i}, \mathcal{U}^{S_i}} = 2\lambda \sum_{i \in \mathfrak{I}} ||\delta U_i||_{\mathcal{U}^{S_i}}^2.$$

Then the value of λ in (2.22) nullifies the derivative of $\mathcal{J}(\lambda) := J(U + \lambda \delta U)$ with respect to λ, thus providing the minimum of the function $\mathcal{J}(\lambda)$. $\qquad \square$

Summarizing, problem (2.17) can be solved in the continuous framework either solving (2.13), (2.18), and (2.19) or following an iterative algorithm such as the steepest descent, in which at each iteration one step is taken along the direction δU computed by (2.20) with a stepsize λ given by (2.22).

The discrete counterparts of these two approaches are presented in section 4.

3. The DFN problem with the extended FEM. In this section, we briefly account for the application of the extended FEM (XFEM) to our context. In the first subsection, we briefly recall from the literature some key points of XFEM; in the second subsection, these ideas are applied to the DFN framework.

3.1. Description of XFEM. The XFEM [3, 8, 4] is a mesh-based numerical technique for the solution of PDEs in variational form, when nonsmooth or discontinuous solutions are considered. The XFEM can reproduce irregularities that are arbitrarily placed in the domain, regardless of the underlying triangulation. The concept at the basis of the XFEM consists in combining the standard finite element approach with the partition of unity method (PUM) [2], in order to overcome the limitations of the finite element approach in dealing with singularities. Customized *enrichment functions* are added to the standard finite element approximation space in order to catch the nonsmooth character of the solution and extend approximation capability.

In what follows only the description of the method in the case of continuous solutions with discontinuous first order derivatives (*weak* discontinuities) is reported, being the only situation of interest in our application. Customizations of the method for other cases can be found in [4, 14].

Given a problem with exact solution H in a domain $\omega \in \mathbb{R}^n$, with a sharp or weak singularity along the interface described by the manifold $S \subset \omega, S \in \mathbb{R}^{n-1}$, let $\mathcal{T}_\delta$ be a conforming triangulation on ω, and let $\mathrm{V}_\delta^{\mathrm{fem}}$ be a finite dimensional trial and test space defined on the elements of $\mathcal{T}_\delta$ and spanned by Lagrangian FE basis functions $\phi_\xi, \xi \in \mathcal{I} = \{1, \ldots, N^{\mathrm{dof}}\}$:

$$(3.1) \qquad \mathrm{V}_\delta^{\mathrm{fem}} = \mathrm{span}\left(\{\phi_\xi(\hat{x})\}_{\xi \in \mathcal{I}}\right).$$

Each basis function ϕ_ξ has compact support Δ_ξ.

In our applications, provided that the edges of the elements in $\mathcal{T}_\delta$ surrounding S match it exactly, the approximate solution of H with standard finite elements has the following form:

$$(3.2) \qquad h_\delta^{\mathrm{fem}}(\hat{x}) = \sum_{\xi \in \mathcal{I}} h_\xi^{\mathrm{fem}} \phi_\xi(\hat{x}),$$

where h_ξ^{fem} is the DOF corresponding to the basis function $\phi_\xi(\hat{x})$. Functions in $\mathrm{V}_\delta^{\mathrm{fem}}$ are continuous and can have discontinuities in the first order derivatives across element edges.

Let us assume Φ is a continuous bounded function on ω, $\Phi \in \mathrm{H}^1(\omega) \cap C^0(\bar{\omega})$ that well approximates the behavior of H in a neighborhood of S called Δ_S. With the XFEM this function is introduced into the standard finite element space, thus defining a new *enriched* functional space with extended approximation capabilities. This can be done by means of the PUM, using the standard finite element shape functions for the definition of a partition of unity. The new enriched functional space is

$$(3.3) \qquad V_\delta^{\mathrm{xfem}} = \mathrm{span}\left(\{\phi_\xi(\hat{x})\}_{\xi \in \mathcal{I}}, \{\phi_\xi(\hat{x})\Phi(\hat{x})\}_{\xi \in \mathcal{J}}\right) \subset \mathrm{H}_0^1(\omega),$$

where we have identified with $\mathcal{J} \subset \mathcal{I}$ the subset of indices of functions ϕ_ξ whose support belongs to Δ_S. DOFs in $\mathcal{J}$ are called enriched DOFs and the corresponding nodes enriched nodes. Typically, as sketched in Figure 3.1 it is

$$(3.4) \qquad \mathcal{J} = \{\xi \in \mathcal{I} : \Delta_\xi \cap S \neq \emptyset\}.$$

Consequently the approximate solution h^{xfem} of the problem with the XFEM is

$$(3.5) \qquad h_\delta^{\mathrm{xfem}}(\hat{x}) = \sum_{\xi \in \mathcal{I}} h_\xi^{\mathrm{xfem}} \phi_\xi(\hat{x}) + \sum_{\xi \in \mathcal{J}} a_\xi^{\mathrm{xfem}} \phi_\xi(\hat{x})\Phi(\hat{x}),$$

where h_ξ^{xfem} and a_ξ^{xfem} are the unknowns related to the standard and enriching basis functions, respectively. Since functions representing the nonsmooth behavior of the solution are now present in the discrete subspace, the nonsmooth behavior of the solution can be reproduced independently of the positioning of elements in $\mathcal{T}_\delta$ with respect to the interface S.

According to (3.4) only a small subset of total elements is enriched and this is a peculiarity of the XFEM if compared to the PUM or other similar methods, for example, the generalized FEM [25, 26]. Elements in $\mathcal{T}_\delta$ may thus have a variable number of enriched nodes. In particular it is possible to group elements in three categories, following the classification used in [14] (see Figure 3.1):

   (i) *standard* elements: no nodes enriched;
   (ii) *reproducing* elements: all nodes enriched;
   (iii) *blending* elements: some nodes enriched.

In reproducing elements, where all the nodes are enriched, the function Φ can be correctly reproduced, providing the desired behavior for the discrete solution. In blending elements, instead, where only some nodes are enriched, spurious terms are introduced in the local discrete space in order to preserve continuity. This may affect the convergence rate of the method compared to the standard FEM. Numerous techniques are suggested in order to prevent this issue, for example, those in [7, 27, 13]. In particular the *modified* XFEM suggested in [13] and adopted here introduces a redefinition of enrichment functions and enriched DOFs in order to correctly account for the contribution of blending elements and recover the standard finite element rate of convergence. We denote by $\widetilde{\Phi}$ and $\widetilde{\mathcal{J}}$ the modified version of Φ and $\mathcal{J}$, respectively, defined as

$$(3.6) \qquad \widetilde{\Phi} = \Phi(\hat{x})R(\hat{x}), \qquad \widetilde{\mathcal{J}} = \{\xi \in \mathcal{I} : \Delta_\xi \cap \Delta_S \neq \emptyset\},$$

where $R(\hat{x}) = \sum_{\xi \in \mathcal{J}} \phi_\xi$. The new enrichment function $\widetilde{\Phi}$ coincides with Φ in reproducing elements where $R = 1$ and vanishes on the boundaries and outside Δ_S, where $R = 0$. Thus anywhere the enrichment function $\widetilde{\Phi}$ is nonzero it is correctly reproduced, avoiding problems related to parasitic terms.

The generalization to other kind of discontinuities follows the same outline described above, with specific redefinition of functional spaces. A comprehensive review of the XFEM/generalized FEM method with details of all implementation aspects is available in [14].

3.2. The discrete DFN problem. With reference to definitions and notation introduced in section 2, we now discuss the application of the XFEM to DFN problems. For brevity we focus here on *closed* interfaces, i.e., traces entirely crossing a
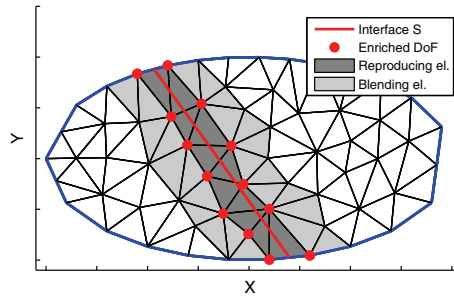
FIG. 3.1. *Selection of nodes in $\mathcal{J}$.*
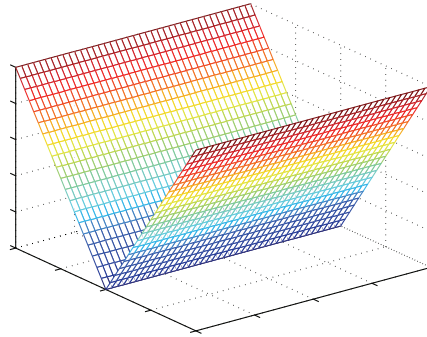
FIG. 3.2. *Function $\Psi(\hat{x})$.*

fracture plane, for example, the one depicted in Figure 3.1. Generalizations to other geometrical configurations of interfaces follow the same outline of this description, requiring, in some cases, the introduction of different enrichment functions. More general cases are considered in [5].

Let us consider a fracture $F \subset \mathbb{R}^2$ that has $\#\mathfrak{M}$ intersections with other fractures in Ω in the traces $S_m \in \mathcal{S}_i$, $m \in \mathfrak{M}$. The starting point for XFEM implementation is a standard finite element setting, defined by a triangulation $\mathcal{T}_\delta^F$ not necessarily conformal to the traces and the discrete test space $V_{F,\delta}^{\text{fem}}$ as defined by (3.1). On F the exact solutions H_F, P_F, and δH_F to (2.13), (2.19), and (2.21), respectively, may have a jump of fluxes (a *weak* discontinuity) across the traces in $\mathcal{S}_i$. The numerical solution of previous equations with XFEM allows the triangulation to be set on each fracture independently of the disposition and number of the traces. This is much more relevant as the number of traces increases or when traces intersect with arbitrary orientations, since in these situations a good quality mesh fitting the interfaces could hardly be produced and would require a huge number of elements, regardless of the required accuracy. Enrichment functions for *weak* discontinuities were introduced in early works with the XFEM, mainly in the context of fracture mechanics. A comprehensive description can be found in [4, 27, 8, 14]. The description of each trace is performed introducing a signed distance function d_m that is defined for $\hat{x} \in F$ as the distance with sign from segments S_m [27, 4]:

$$d_m(\hat{x}) = \|\bar{x} - \hat{x}\| \frac{\hat{n}_S \cdot (\bar{x} - \hat{x})}{\|\hat{n}_S \cdot (\bar{x} - \hat{x})\|},$$

where $\bar{x}$ is the projection of $\hat{x}$ on S_m and $\hat{n}_S$ the fixed unit normal vector to S_m. The enrichment functions are built starting from the signed distance functions. For a closed interface we use the enrichment function Ψ_m defined as $\Psi_m(\hat{x}) = |d_m(\hat{x})|$. Clearly Ψ_m is a continuous function, but its first order derivatives have a jump across S_m, thus introducing the required nonsmooth behavior in the approximation (Figure 3.2). The sets of enriched DOFs, $\mathcal{J}_m$, are defined according to (3.4) for each trace.

In order to avoid problems related to blending elements, the XFEM modified version [13] is used. Functions $\widetilde{\Psi}_m$ and sets $\widetilde{\mathcal{J}}_m$ are built starting from Ψ_m and $\mathcal{J}_m$ according to definition (3.6). The discrete approximation space is thus

$$(3.7) \qquad V_{F,\delta}^{\text{xfem}} = \text{span}\left(\{\phi_\xi(\hat{x})\}_{\xi \in \mathcal{I}}, \{\phi_\xi(\hat{x})\Phi_m(\hat{x})\}_{m \in \mathfrak{M}, \xi \in \mathcal{J}_m}\right) \subset \mathrm{H}_0^1(\omega),$$

and the discrete solution is

$$(3.8) \qquad h_{F,\delta}^{\mathrm{xfem}}(\hat{x}) = \sum_{\xi \in \mathcal{I}} h_\xi \phi_\xi(\hat{x}) + \sum_{m \in \mathfrak{M}} \sum_{\xi \in \widetilde{\mathcal{J}}_m} a_\xi^m \phi_\xi(\hat{x}) \widetilde{\Psi}_m(\hat{x}).$$

We remark the additivity of the previous formula with respect to the interfaces: the previous expression does not depend on where traces are located, how close they are to each other, or whether they do intersect each other, nor on which elements the enriched functions are defined.

The numerical integration of nonsmooth functions is performed on subdomains where the restriction of basis functions is regular. A Gauss quadrature rule is used, adopting the number of integration nodes required by the polynomial degree of the integrands.

4. Discrete formulation. In this section we provide a discrete formulation of problem (2.17). For simplicity, we assume in this section homogeneous Dirichlet boundary conditions, i.e., $H_D = 0$. All the results can be extended to the general case $H_D \neq 0$; see Remark 4.2. For simplicity of notation again, in this section, given two (or more) vectors $x \in \mathbb{R}^p$ and $y \in \mathbb{R}^q$, we will write (x, y) denoting the vector $(x^T, y^T)^T \in \mathbb{R}^{p+q}$.

Under assumptions (2.16), the minimum of the functional $J(U)$ is characterized by conditions involving a fractional power of the Laplace operator on the traces. Hence, we develop our numerical method for the approximation of the solution adopting the following choices:

$$(4.1) \qquad \mathcal{U}^S = \mathrm{L}^2(S), \qquad \mathcal{H}^S = \mathrm{L}^2(S) \qquad \forall S \in \mathcal{S}.$$

Remark 4.1. We remark that with these choices the assumption of disconnected traces can be removed. This is due to the following property of the L^2-norm: if S_1 and S_2 are two possibly connected traces, then $\| \cdot \|_{\mathrm{L}^2(S_1 \cup S_2)}^2 = \| \cdot \|_{\mathrm{L}^2(S_1)}^2 + \| \cdot \|_{\mathrm{L}^2(S_2)}^2$ (see also Remark 2.1).

For all $i \in \mathfrak{I}$, let $J_i \subset \mathfrak{I}$ be the subset of indices such that for $j \in J_i$, the fracture F_j shares a trace with F_i. Furthermore, $\forall i \in \mathfrak{I}$ and $\forall S \in \mathcal{S}_i$, let us fix a finite dimensional subspace of $\mathcal{U}^S$ for the discrete approximation u_i^S of the control variable U_i^S. With similar notation let us also denote by h_i the discrete approximation of H_i. Let us introduce a basis $\{\psi_{i,k}^S\}_{k=1,\ldots,N_{i,S}}$ for this subspace, so that we write

$$u_i^S = \sum_{k=1}^{N_{i,S}} u_{i,k}^S \psi_{i,k}^S \quad \forall i \in \mathfrak{I}, S \in \mathcal{S}_i.$$

Replacing these expressions in (2.15), using the L^2-norm and $C_i^S h_i = h_{i|_S}$, we get

$$(4.2) \qquad J(u) = \frac{1}{2} \sum_{i \in \mathfrak{I}} \sum_{S \in \mathcal{S}_i} \left(\int_S \left(\sum_{k=1}^{N_i} h_{i,k} \phi_{i,k|_S} - \sum_{k=1}^{N_j} h_{j,k} \phi_{j,k|_S} \right)^2 \mathrm{d}\gamma \right.$$

$$\left. + \int_S \left(\sum_{k=1}^{N_{i,S}} u_{i,k}^S \psi_{i,k}^S + \sum_{k=1}^{N_{j,S}} u_{j,k}^S \psi_{j,k}^S \right)^2 \mathrm{d}\gamma \right).$$

For all $i \in \mathfrak{I}$ and $S \in \mathcal{S}_i$, let us introduce the subset $K_{i,S} \subseteq \{1, \ldots, N_i\}$ of indices k of functions $\phi_{i,k}$ whose support has a nonempty intersection with S. The first integral in (4.2) is rewritten as

$$I_{ij}^{S,h} = \sum_{k \in K_{i,S}} h_{i,k}^2 \int_S {\phi_{i,k}}_{|S}^2 \, \mathrm{d}\gamma + 2 \sum_{k,\ell \in K_{i,S}} h_{i,k} h_{i,\ell} \int_S {\phi_{i,k}}_{|S} {\phi_{i,\ell}}_{|S} \, \mathrm{d}\gamma + \sum_{k \in K_{j,S}} h_{j,k}^2 \int_S {\phi_{j,k}}_{|S}^2 \, \mathrm{d}\gamma$$

$$+ 2 \sum_{k,\ell \in K_{j,S}} h_{j,k} h_{j,\ell} \int_S {\phi_{j,k}}_{|S} {\phi_{j,\ell}}_{|S} \, \mathrm{d}\gamma - 2 \sum_{k \in K_{i,S}} \sum_{\ell \in K_{j,S}} h_{i,k} h_{j,\ell} \int_S {\phi_{i,k}}_{|S} {\phi_{j,\ell}}_{|S} \, \mathrm{d}\gamma.$$

Let us introduce vectors $h_i \in \mathbb{R}^{N_i}$, $h_i = (h_{i,1}, \ldots, h_{i,N_i})^T$, $i \in \mathfrak{I}$, and setting $N^F = \sum_{i \in \mathfrak{I}} N_i$, let $h \in \mathbb{R}^{N^F}$ be obtained concatenating, for $i \in \mathfrak{I}$, vectors h_i. Hence from now on, besides denoting the discrete solution, h_i will also denote the vector of corresponding DOFs.

Next, for all $i \in \mathfrak{I}$, $S \in \mathcal{S}_i$ let us define matrices $M_i^S \in \mathbb{R}^{N_i \times N_i}$ and (for $j \in J_i$) $M_{ij}^S \in \mathbb{R}^{N_i \times N_j}$ as

$$(M_i^S)_{k\ell} = \int_S {\phi_{i,k}}_{|S} {\phi_{i,\ell}}_{|S} \, \mathrm{d}\gamma, \qquad (M_{ij}^S)_{k\ell} = \int_S {\phi_{i,k}}_{|S} {\phi_{j,\ell}}_{|S} \, \mathrm{d}\gamma.$$

With these definitions, the first integral in (4.2) is written in compact form as

$$(4.3) \qquad\qquad I_{ij}^{S,h} = h_i^T M_i^S h_i + h_j^T M_j^S h_j - 2 h_i^T M_{ij}^S h_j.$$

Let us turn to the second integral in (4.2). For a convenient compact form of this second integral, let us consider a different numbering of functions u_i^S induced by the trace numbering. Let $S = S_m$ be a given trace with $c_m = (i,j)$ (hence $i < j$). We denote by u_m^- the control function related to the mth trace and corresponding to fracture F_i and by u_m^+ the control function related to the same trace and corresponding to the other fracture, F_j. This numbering induces a different numbering also on the basis functions $\psi_{i,k}^S$, $\psi_{j,k}^S$ which can be labeled as $\psi_{m,k}^-$, $\psi_{m,k}^+$, respectively, and accordingly we set $N_m^+ = N_{i,S}$, $N_m^- = N_{j,S}$.

Then we have, for $\star = -$ or $+$,

$$u_m^\star = \sum_{k=1}^{N_m^\star} u_{m,k}^\star \psi_{m,k}^\star \quad \forall m \in \mathfrak{M}.$$

Now, let us introduce the vectors $u_m^\star \in \mathbb{R}^{N_m^\star}$, $u_m^\star = (u_{m,1}^\star, \ldots, u_{m,N_m^\star}^\star)^T$, $m \in \mathfrak{M}$, $\star = -, +$, and setting $N^T = \sum_{m \in \mathfrak{M}} (N_m^- + N_m^+)$ we define $u \in \mathbb{R}^{N^T}$ as

$$u = (u_1^-, u_1^+, \ldots, u_{\#\mathfrak{M}}^-, u_{\#\mathfrak{M}}^+).$$

Let us also define the following matrices:

$$\mathcal{M}_m^\star \in \mathbb{R}^{N_m^\star \times N_m^\star}, \qquad (\mathcal{M}_m^\star)_{k\ell} = \int_S \psi_{m,k}^\star \psi_{m,\ell}^\star \, \mathrm{d}\gamma, \qquad m \in \mathfrak{M}, \quad \star = -, +$$

$$\mathcal{M}_m^\pm \in \mathbb{R}^{N_m^- \times N_m^+}, \qquad (\mathcal{M}_m^\pm)_{k\ell} = \int_S \psi_{m,k}^- \psi_{m,\ell}^+ \, \mathrm{d}\gamma.$$

The second integral in (4.2), after some straighforward algebraic manipulation, is rewritten as

$$I_{ij}^{S,u} = \sum_{k=1}^{N_m^-} {u_{m,k}^-}^2 \int_S {\psi_{m,k}^-}^2 \, \mathrm{d}\gamma + 2 \sum_{k=1}^{N_m^-} \sum_{\ell=1}^{N_m^-} u_{m,k}^- u_{m,\ell}^- \int_S \psi_{m,k}^- \psi_{m,\ell}^- \, \mathrm{d}\gamma + \sum_{k=1}^{N_m^+} {u_{m,k}^+}^2 \int_S {\psi_{m,k}^+}^2 \, \mathrm{d}\gamma$$

$$+ 2 \sum_{k=1}^{N_m^+} \sum_{\ell=1}^{N_m^+} u_{m,k}^+ u_{m,\ell}^+ \int_S \psi_{m,k}^+ \psi_{m,\ell}^+ \, \mathrm{d}\gamma + 2 \sum_{k=1}^{N_m^-} \sum_{\ell=1}^{N_m^+} u_{m,k}^- u_{m,\ell}^+ \int_S \psi_{m,k}^- \psi_{m,\ell}^+ \, \mathrm{d}\gamma$$

and in compact form as

$$(4.4) \qquad I_{ij}^{S,u} = (u_m^-)^T \, \mathcal{M}_m^- \, u_m^- + (u_m^+)^T \, \mathcal{M}_m^+ \, u_m^+ + 2(u_m^-)^T \, \mathcal{M}_m^\pm \, u_m^+.$$

We can now write the whole functional $J(u)$ in matrix form properly assembling the previous matrices into a single one and resorting to vectors h and u. Let $G^h \in \mathbb{R}^{N^F \times N^F}$ and $G^u \in \mathbb{R}^{N^T \times N^T}$ be defined blockwise as follows: for $i \in \mathfrak{I}$, $m \in \mathfrak{M}$ we set

$$G_{ii}^h = \sum_{S \in \mathcal{S}_i} M_i^S, \qquad G_{ij}^h = -M_{ij}^S \text{ for } j \in J_i,$$

$$\mathcal{M}_m = \begin{pmatrix} \mathcal{M}_m^- & \mathcal{M}_m^\pm \\ (\mathcal{M}_m^\pm)^T & \mathcal{M}_m^+ \end{pmatrix}, \qquad G^u = \text{diag}(\mathcal{M}_1, \dots, \mathcal{M}_{\#\mathfrak{M}}).$$

Since obviously $(M_{ij}^S)^T = M_{ji}^S$, matrix G^h is symmetric. The same property clearly holds true for G^u. With these definitions, the functional $J(u)$ can be rewritten as

$$J(u) = \frac{1}{2} h^T G^h h + \frac{1}{2} u^T G^u u.$$

Now, let us turn our attention to the constraints, writing the algebraic counterparts of operators A_i, B_i in (2.14): overloading notation, we let $A_i \in \mathbb{R}^{N_i \times N_i}$ and $B_i \in \mathbb{R}^{N_i \times N_{\mathcal{S}_i}}$ with $N_{\mathcal{S}_i} = \sum_{S \in \mathcal{S}_i} N_{i,S}$ also denote the matrices defining the algebraic operators as follows. We set

$$(4.5) \qquad (A_i)_{k\ell} = \int_{F_i} \nabla \phi_{i,\ell} \nabla \phi_{i,k} \, dF_i, \quad \left(B_i^{S_m}\right)_{k\ell} = \int_{S_m} \phi_{i,k\,|\,S_m} \psi_{m,\ell}^\star \, d\gamma,$$

where, recalling that $I_{S_m} = \{i, j\}$, we take $\star = -$ if $i < j$ or $\star = +$ otherwise. Matrices $B_i^{S_m}$, $S_m \in \mathcal{S}_i$, are then grouped rowwise to form the matrix B_i, which acts on a column vector u_i containing all the control DOFs corresponding to traces of F_i. Vector u_i is obtained appending the blocks $u_m^\star$ in the same order used for assembling B_i, as the action of a suitable operator $R_i : \mathbb{R}^{N^T} \mapsto \mathbb{R}^{N_{\mathcal{S}_i}}$ such that $u_i = R_i u$. Hence, constraints (2.14) lead to the algebraic equations

$$(4.6) \qquad A_i h_i - B_i R_i u = \tilde{q}_i, \qquad i \in \mathfrak{I},$$

where $\tilde{q}_i$ accounts for the term q_i in (2.14) and for the weak discrete imposition of boundary conditions. Letting $w = (h, u) \in \mathbb{R}^{N^F + N^T}$ and defining

$$A = \text{diag}(A_1, \dots, A_{\#\mathfrak{I}}) \in \mathbb{R}^{N^F \times N^F}, \qquad B = \begin{pmatrix} B_1 R_1 \\ \vdots \\ B_{\#\mathfrak{I}} R_{\#\mathfrak{I}} \end{pmatrix} \in \mathbb{R}^{N^F \times N^T},$$

$$(4.7) \qquad C = (A \quad -B) \in \mathbb{R}^{N^F \times N^F + N^T}, \qquad G = \text{diag}(G^h, \ G^u),$$

the overall problem reads

$$(4.8) \qquad\qquad \min_w \ \frac{1}{2} w^T G w,$$

$$(4.9) \qquad\qquad \text{s.t. } Cw = \tilde{q}.$$

Hence the problem is a quadratic programming (QP) problem with equality constraints. First order necessary conditions for a point w^* to be a solution to (4.8)–(4.9) are given by the Karush–Khun–Tucker conditions (see, e.g., [21]):

$$(4.10) \qquad \mathcal{A} = \begin{pmatrix} G & C^T \\ C & 0 \end{pmatrix}, \qquad \mathcal{A} \begin{pmatrix} w^* \\ -p^* \end{pmatrix} = \begin{pmatrix} 0 \\ \tilde{q} \end{pmatrix},$$

where p^* is the vector of Lagrange multipliers.

Remark 4.2. The results presented here do not rely on the assumption of homogeneous Dirichlet boundary conditions. If nonhomogeneous Dirichlet conditions are taken into account, the quadratic functional in (4.8) also contains a linear term; correspondingly, the right-hand side of (4.10) has a nonzero block, and the structure of the problem is therefore the same.

For further discussion, we recall the following classical result concerning solution of equality constrained QPs of the form (4.8)–(4.9); see, for example, [21]. Referring to problem (4.8)–(4.9), let n and p denote the dimension of w and the number of constraints, respectively, so that $G \in \mathbb{R}^{n \times n}$ and $C \in \mathbb{R}^{p \times n}$.

THEOREM 4.3. *Let C have full row rank and assume that the matrix $Z^T G Z$ is positive definite, where Z is a $n \times (n - p)$ matrix whose columns are a basis of the null space of C. Then the matrix $\mathcal{A}$ defined in* (4.10) *is nonsingular and the vector w^* satisfying* (4.10) *is the unique global solution of problem* (4.8)–(4.9).

Proof of existence and uniqueness of the solution to the discrete counterpart of problem (2.17) is now a direct application of Theorem 4.3.

THEOREM 4.4. *Let us consider the discrete formulation* (4.8)–(4.9) *to the problem of subsurface flow in a DFN with G and C defined as in* (4.7). *Then, the solution exists and is unique and coincides with the solution to* (4.10).

Proof. First, let us observe that G is symmetric positive semidefinite as for any $w = (h, u)$ we straightforwardly have $w^T G w \geq 0$. Furthermore, since all A_i are nonsingular, due to standard properties of finite element discretizations, A is nonsingular as well and C has full row rank. As $\mathrm{rank}(C) = N^F$ we have $\dim(\ker(C)) = N^T$. Let $z_1, \ldots, z_{N^T} \in \mathbb{R}^{N^F + N^T}$ be vectors forming a basis of $\ker(C)$. Then $\forall z_k$, let us partition $z_k = (z_k^h, z_k^u)$ with $z_k^h \in \mathbb{R}^{N^F}$ and $z_k^u \in \mathbb{R}^{N^T}$. We have $A z_k^h = B z_k^u$, and thus z_k has the form $(A^{-1} B z_k^u, z_k^u)$. In particular, take $z_k^u = e_k$, where e_k is the kth vector of the canonical basis of $\mathbb{R}^{N^T}$, hence $z_k = (A^{-1} B e_k, e_k)$. Let us compute $y = G z_k = (G^h A^{-1} B e_k, G^u e_k)$. Let $e_{N^F + s}$ be a vector of the canonical basis of $\mathbb{R}^{N^F + N^T}$ with $s \geq 1$. We have $y_{N^F + s} = e_{N^F + s}^T G z_k = e_s^T G^u e_k$ with $e_s \in \mathbb{R}^{N^T}$. In particular, taking $s = k$, we have

$$(4.11) \qquad y_{N^F + k} = e_k^T G^u e_k = \int_S {\psi_{i,\ell}^S}^2 \, d\gamma$$

for some $i \in \mathfrak{I}$ and some $1 \leq \ell \leq N_{i,S}$. Since the integral in (4.11) is nonzero, we have at least one component of $G z_k$ different from zero. Hence we have proved that for any vector $z \in \ker(C)$, we have $G z \neq 0$ (unless $z = 0$), hence $z \notin \ker(G)$. This proves that $\ker(G) \cap \ker(C) = \{0\}$. Now let Z be the matrix whose columns are given by the basis vectors z_k previously introduced. Since G is positive semidefinite we have, for any $y \in \mathbb{R}^{N^F + N^T}$, $y^T G y \geq 0$ and $y^T G y = 0$ if and only if $y \in \ker(G)$ (see, e.g., [16]). Let $v \in \mathbb{R}^{N^T}$ be an arbitrary vector, $v \neq 0$. Since $Z v \in \ker(C)$ and $\ker(G) \cap \ker(C) = \{0\}$, we have $Z v \notin \ker(G)$ and so $v^T Z^T G Z v > 0$. This proves positive definiteness of $Z^T G Z$. Applying Theorem 4.3, the thesis is proved. ☐

4.1. Computing numerical solutions. Saddle point system (4.10) represents a possible approach for obtaining a numerical solution. For a DFN of moderate size, sparse (even direct) solvers can be used efficiently to compute a solution to (4.10). Nevertheless, when the DFN system is composed of a huge number of fractures, even if poor discretizations are introduced on each fracture, solving the linear system may be a quite demanding task and parallel computing has to be taken into account. If this is the case, instead of assembling the linear system and splitting information and operations among processors/cores, a gradient-based method such as the basic one depicted in what follows can be taken into account. The following numerical method arises from the discretization of the steepest descent method briefly described at the end of subsection 2.2. At step k, given u^k, let us compute h_i^k as the solution to (4.6) and p_i^k as the solution to

$$(4.12) \qquad A_i^T p_i^k = G_{ii}^h h_i^k + \sum_{j \in J_i} G_{ij}^h h_j^k \qquad \forall i \in \mathfrak{I}.$$

Then, we define a vector δu_i^k componentwise as the $\mathrm{L}^2(\mathcal{S}_i)$ projection of the function $p_i^k + \prod_{S_m \in \mathcal{S}_i}((u_m^-)^k + (u_m^+)^k)$ against basis functions. Nodal interpolation can be taken in the case of Lagrangian basis functions. Then, we move along direction δu^k with a stepsize

$$(4.13) \quad \lambda_k = -\frac{\sum_{i \in \mathfrak{I}} (\delta u_i^k)^T \delta u_i^k}{\frac{1}{2} \sum_{i \in \mathfrak{I}} \sum_{S_m \in \mathcal{S}_i} \left(\|\delta h_i{}^k_{|S_m} - \delta h_j{}^k_{|S_m}\|^2_{\mathrm{L}^2(S_m)} + \|(u_m^-)^k + (u_m^+)^k\|^2_{\mathrm{L}^2(S_m)} \right)},$$

where δh_i^k is the solution to

$$(4.14) \qquad A_i \delta h_i^k = B_i \delta u_i^k \qquad \forall i \in \mathfrak{I}.$$

The corresponding algorithm is the following.

ALGORITHM 4.5.
1. *Set $k = 0$ and initial guess for control variable u^0;*
2. *compute $h^0 = h(u^0)$ solving (4.6) on each fracture;*
3. *Do*
    3.1 *compute p^k solving on each fracture the dual problem (4.12);*
    3.2 *compute δu^k and solve (4.14) to get δh;*
    3.3 *evaluate λ^k according to (4.13) and update $u^{k+1} = u^k + \lambda^k \delta u^k$;*
    3.4 *compute $h^{k+1} = h^k + \lambda^k \delta h^k$*
    3.5 *$k = k + 1$*
    while *stopping criterion* is not satisfied.

Remark 4.6. Algorithm 4.5, which is the discretization of the infinite dimensional steepest descent method, is equivalent to the application of the steepest descent method to the finite dimensional problem (4.8)–(4.9).

Each iteration of Algorithm 4.5 essentially requires the solution of (4.12) and (4.14), whereas it is not necessary to solve the primal equation (4.6) at each iteration, because, thanks to linearity, the new value h^{k+1} for the numerical hydraulic head can be computed as shown in Step 3.4 Nevertheless, in practical computations, it is advisable to periodically replace Step 3.4 with the computation of h^{k+1} via the primal equation, in order to improve numerical stability.

We end this section by highlighting that solutions to problems (4.12) and (4.14) can be obtained by decoupling the computation among fractures. This point makes the method appealing when parallelization comes into play, as this approach turns out to be highly parallelizable in a very natural way, by distributing fractures among

processors and involving a moderate exchange of data. This approach is suitable for massively parallel computers and GPU-based computers.

5. Numerical results. In this section we present some preliminary results which aim to show the viability and effectiveness of the method proposed here in circumventing any kind of problem concerning mesh generation on the whole DFN.

Two test problems have been considered here. In Problem 1 the numerical simulations are performed both with standard finite elements on conforming grids aligned to a trace and with extended finite elements with a trace crossing mesh elements. Numerical results are compared to the known exact solution. In Problem 2 a more complex domain is considered. In both tests, traces entirely crossing a fracture are considered. The application of the method to more complex DFN configurations is shown in [5]. Triangular meshes and first order finite elements are used in all the tests. Let $V_{i,\delta}$ be the discrete enriched finite element space on the fracture $F_i \ \forall i \in \mathfrak{I}$, defined according to (3.7). Let $\mathcal{U}_\delta \subset \mathcal{U}$ be the discrete space for the control functions. The space $\mathcal{U}_\delta$ is here defined as the space of the piecewise linear functions on the traces $S_m, \ m \in \mathfrak{M}$; the nodes of the one-dimensional mesh on each trace are given by the intersections of the 2D mesh on the corresponding fracture with the trace itself. If an edge of the 2D mesh lies on the trace, the endpoints of the edge are taken as nodes of the one-dimensional mesh.

In the presentation of numerical results the following convention is used:
- FEM: our optimization approach on standard finite element meshes without enrichments; meshes are aligned along the traces (Figure 5.1, left). For Problem 1 the same mesh is used in all the fractures. This method is used to compare our results with those obtained on a conforming mesh, in which it is ensured that the minimum of J equals 0.
- XFEM: extended finite elements are used and the meshes in all the fractures do not match along the traces (Figure 5.1, right). In this case the minimum of functional J computed with the discrete solutions is in general $\neq 0$.

In all tests we computed the numerical solution both using the gradient method and solving the linear system (4.10). When the gradient method was applied, we started from a null control u^0. Both the overall linear system (4.10) and the smaller dimension systems involved in (4.12) and (4.14) have been solved with the MATLAB built-in direct solver.

Depending on the choices of the mesh on each fracture F_i, the minimum of functional $J(u)$ can be different from zero. In Algorithm 4.5 the following stopping criteria have been used:

$$(5.1) \qquad J(u^k) - J(u^{k+1}) < \text{tol}_1 \qquad \text{or} \qquad \frac{J(u^k) - J(u^{k+1})}{J(u^{k+1})} < \text{tol}_2.$$

In the results here reported we used $\text{tol}_1 = 10^{-15}$ and $\text{tol}_2 = 10^{-3}$.

5.1. Problem 1. Let us define $\Omega = F_1 \cup F_2$, where $\mathbf{x} = (x, y, z)$, and F_1 and F_2 are given by

$$F_1 = \left\{ \mathbf{x} \in \mathbb{R}^3 : x \in (-1, 1), y \in (0, 1), z = 0 \right\},$$
$$F_2 = \left\{ \mathbf{x} \in \mathbb{R}^3 : x = 0, \ y \in (0, 1), \ z \in (-1, 1) \right\}.$$

Let $S = F_1 \cap F_2$. The problem is set as follows:

$$(5.2) \qquad -\Delta H = q \qquad \text{in } \Omega \backslash \text{S}$$

with homogeneous Dirichlet boundary conditions on all the boundary $\partial\Omega$. The forcing function q is defined as follows:

$$q(\mathbf{x}) = \begin{cases} 6(y - y^2)|x| - 2(|x^3| - |x|) & \text{on } F_1, \\ -6(y - y^2)|z| + 2(|z^3| - |z|) & \text{on } F_2, \end{cases}$$

and the exact solution is given by

$$H(\mathbf{x}) = \begin{cases} -y(1 - y)|x|(x^2 - 1) & \text{on } F_1, \\ y(1 - y)|x|(x^2 - 1) & \text{on } F_2. \end{cases}$$

Figure 5.1, left, shows a mesh used for the fractures F_1 and F_2 using standard finite elements, whereas the right shows the domain and, on each fracture, the mesh used with the extended finite elements. Note that in the second case the two meshes on F_1 and F_2 are not conforming. Both figures refer to intermediate meshes, corresponding to meshsize $\delta_{max} = 0.06$, where $\delta_{max} = 0.25$ and $\delta_{max} = 0.016$ are the meshsizes of the coarsest and finest grids used, respectively.

Figure 5.2 displays the solutions on F_1 and F_2 obtained with XFEM on the intermediate grid. The same solution is also represented in Figure 5.1, right, with a colorbar. Near the trace the numerical solution is plotted on the subelements generated by cutting XFEM elements along traces. It can be noted that the correct nonsmooth behavior of the solution is caught by XFEM enrichments even if element edges do not match the trace. Figure 5.3 shows the behavior of L^2 and H^1 error norms with respect to the meshsize δ_{max} during a uniform mesh refinement process. The
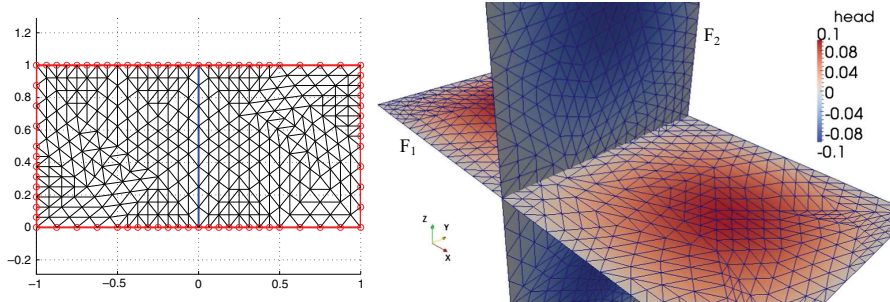

FIG. 5.1. *Problem 1: Left: standard FEM conforming mesh on each fracture; right: domain description with XFEM meshes and solution h in colorbar.*
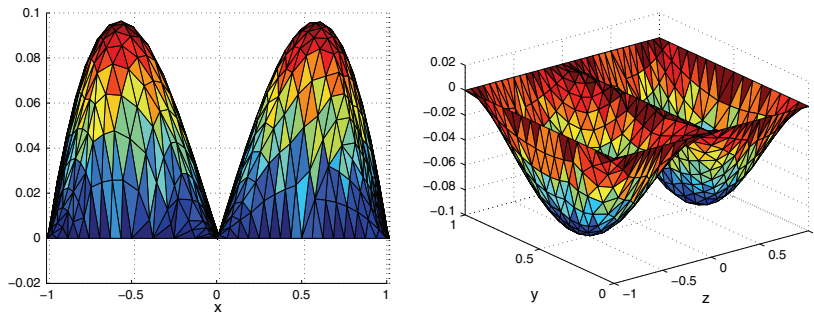

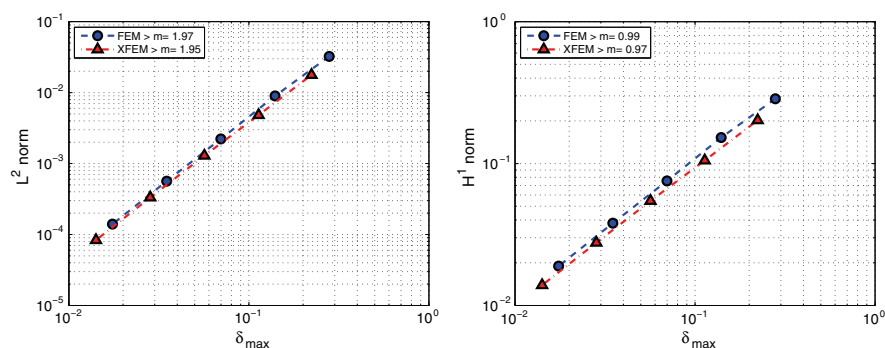FIG. 5.2. *Problem 1: Solution with XFEM on fracture F_1 (left) and F_2 (right) for $\delta_{max} = 0.06$.*

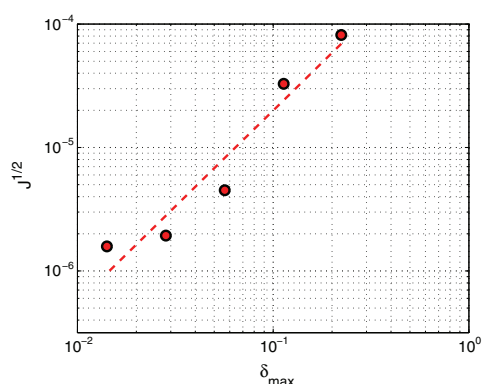FIG. 5.3. *Problem* 1: L^2 *(left) and* $H^1(\Omega)$ *(right) error norms under grid refinement.*

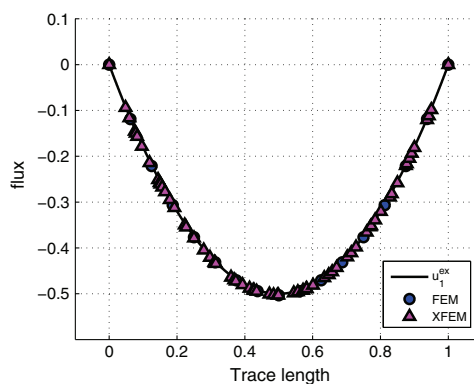FIG. 5.4. *Problem* 1: *Minimum of* $\sqrt{J}$ *under grid refinement.*

FIG. 5.5. *Problem* 1: *Control variable and exact solution (intermediate grid).*

slopes m of the curves, reported in the legend of each figure, agree with the expected values for P^1 elements even in the case of XFEM.

Remark 5.1. For this test problem we have $H(\mathbf{x}) \notin \mathrm{H}^2(F_i)$, $i = 1, 2$, whereas $H(\mathbf{x}) \in \mathrm{H}^2(f)$, f being any one of the four subfractures in which F_1 and F_2 are divided by the trace. As described in [15, 29], this regularity is enough to provide the convergence orders of Figure 5.3, which are the theoretical ones for $H(\mathbf{x}) \in \mathrm{H}^2(F_i)$.

Figure 5.4 displays the minimum value of $\sqrt{J}$ as a function of the meshsize on nonconforming meshes. In the XFEM case the target minimum of the functional is different from zero and, as expected, its value depends on the meshsize, while this is not the case for the standard FEM, since the minimum of the functional can vanish independently of the meshsize.

In Figure 5.5 the exact value of $\left[\!\left[\frac{\partial H_1}{\partial \hat{\nu}_S^1}\right]\!\right]$ is compared with the computed values of the control variable u_1 obtained on the intermediate grids, both with FEM and with XFEM. The figure clearly shows a very good agreement between all the values. The norm of the flux mismatch on the trace, i.e., $\|u_1 + u_2\|_{\mathrm{L}^2(S)}$, has been computed with both approaches, obtaining $\|u_1 + u_2\|_{\mathrm{L}^2(S)} \simeq 10^{-16}$ with FEM and $\|u_1 + u_2\|_{\mathrm{L}^2(S)} = 3.1\,10^{-8}$ with XFEM.

Remark 5.2. The vanishing of the minimum value of the functional with standard FEM does not correspond to a significantly better approximation of the global solution, as we can argue by comparing the errors in the solution in Figure 5.3, where
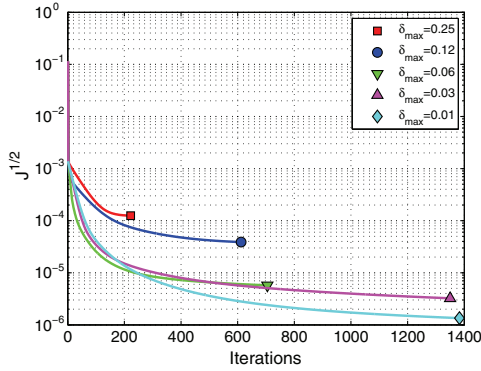
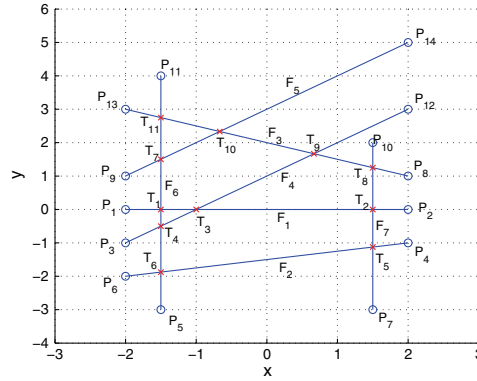FIG. 5.6. *Problem 1: Functional trend against iterations with XFEM (five grids).*

FIG. 5.7. *Problem 2: Fractures configuration, projection on $x - y$ plane.*

we can see that the errors corresponding to the same meshsize are comparable in the FEM and XFEM cases, with both L^2- and H^1-norms. As seen in Figure 5.5, the accuracy of the fluxes on the trace are comparable. The vanishing minimum value of J for FEM is only related to a better satisfiability of the matching conditions between the approximated solutions on the fractures, and the accuracy of the overall solution is comparable for XFEM and FEM.

In Figure 5.6 the behavior of $\sqrt{J}$ during the minimization process attained by the gradient method is shown. As expected the functional related to the XFEM solution reaches a plateau corresponding to a nonvanishing value when one of the stopping criteria in (5.1) is satisfied. As shown in Figure 5.6, mesh refinement can reduce the final functional value.

No effort has been spent here for improving convergence properties of the minimization process, as our main target is proving viability of the approach. Many improvements in the optimization process are possible; future work will be devoted to this issue. Nevertheless, despite the number of iterations required by the gradient method, the computational cost of each iteration is small, as it essentially requires the solution of the state equations on each fracture. This aspect itself makes the method appealing when parallelization comes into play.

5.2. Problem 2. In the second test problem the proposed method is applied to a DFN composed by seven rectangular fractures. Figure 5.7 shows the intersections of the fractures with the plane $z = 0$. All the fractures have z ranging from 0 to 1. In Figure 5.7, P_n, $n = 1, \ldots, 14$, denotes the starting and ending points of the intersections; F_i, $i = 1, \ldots, 7$, the intersection of the fractures with $z = 0$; and T_m, $m = 1, \ldots, 11$, the intersections of the traces S_m with $z = 0$. The 3D DFN configuration is shown in Figure 5.8.

The problem is set as follows:

$$(5.3) \qquad -\Delta H = 0 \qquad \text{in } \Omega \setminus \mathcal{S},$$

$$(5.4) \qquad H_{|\Gamma_D} = y + \sqrt{z} \qquad \text{on } \Gamma_D,$$

$$(5.5) \qquad \frac{\partial H}{\partial \hat{\nu}} = 0 \qquad \text{on } \Gamma_N,$$

where $\mathcal{S} = \bigcup_{m=1,\ldots,11} S_m$, Γ_D is the set of the edges along the z direction intersecting $z = 0$ in the points P_{13}, P_9, P_1, P_3, P_6, P_5, and P_7, whereas Γ_N is the set of
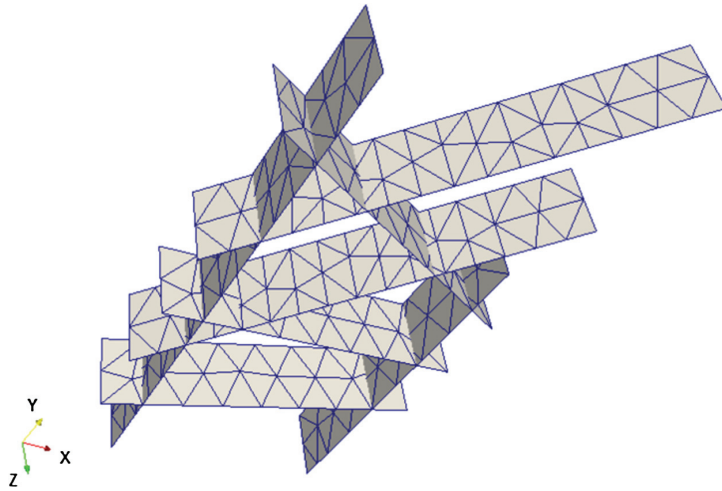
FIG. 5.8. *Problem 2: Fracture configuration and meshes.*

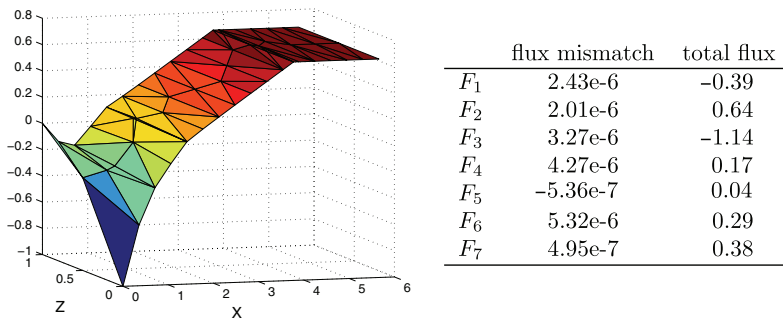|	flux mismatch	total flux
F_1	2.43e-6	−0.39
F_2	2.01e-6	0.64
F_3	3.27e-6	−1.14
F_4	4.27e-6	0.17
F_5	−5.36e-7	0.04
F_6	5.32e-6	0.29
F_7	4.95e-7	0.38

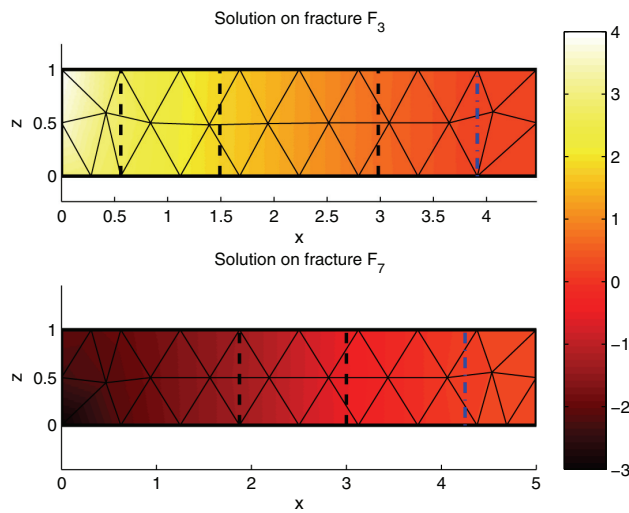FIG. 5.9. *Problem 2: Solution on fracture F_4 (left) and flux mismatch on the fractures (right).*

FIG. 5.10. *Problem 2: Solution on F_3 (top) and F_7 (bottom).*

all the other boundaries of the fractures. The computing mesh used is depicted in Figure 5.8. We remark that the meshes on the fractures are independently generated with meshsize $\delta_{\max} = 0.39$ without requiring any conformity constraint along the traces.

The solution is shown on some selected fractures. In Figure 5.9 the solution on fracture F_4 is shown. Here, in order to better display the enriched numerical solution, it is plotted, rather than on the actual computing elements, on subelements generated by splitting the computing elements along traces.

Figure 5.10 shows, using a colormap, solutions on fractures F_3 and F_7. Here, the mesh depicted is the actual computing mesh. The vertical dashed lines correspond to traces. The rightmost dash-dot vertical line is a common trace between the two fractures. Nonconformity of meshes is clearly shown in the figure. Finally, in the table on the right of Figure 5.9 we report, for each fracture F_i, $i = 1, \ldots, 7$, the flux mismatch and total flux, computed as $\sum_{S \in \mathcal{S}_i} \int_S u_i^S + u_j^S \, d\gamma$ and $\sum_{S \in \mathcal{S}_i} \int_S u_i^S \, d\gamma$, respectively. The overall flux mismatch on the whole DFN is 8.14e-6.

6. Conclusions. In this paper we propose a new approach to DFN simulation, which does not need any kind of conformity along the traces for the meshes introduced on the fractures. The method proposed thus circumvents all the difficulties typically related to mesh generation processes of partially or totally conforming grids. This novel approach is based on a PDE-constrained optimization problem and is developed in order to be easily parallelized on massively parallel or GPU-based or hybrid parallel computers. The key point which makes the method suitable for a parallel approach is that the global solution is obtained through the resolution of many small local problems that require a moderate exchange of data among fractures. Some preliminary numerical simulations prove the viability of the approach. A detailed analysis of the performance of the method on more complex fracture configurations is proposed in [5].

REFERENCES

[1] P. M. ADLER, *Fractures and Fracture Networks*, Kluwer Academic, Dordrecht, Netherlands, 1999.
[2] I. BABUŠKA AND J. M. MELENK, *The partition of unity method*, Internat. J. Numer. Methods Engrg., 40 (1997), pp. 727–758.
[3] T. BELYTSCHKO AND T. BLACK, *Elastic crack growth in finite elements with minimal remeshing*, Internat. J. Numer. Methods Engrg., 45 (1999), pp. 601–620.
[4] T. BELYTSCHKO, N. MÖES, S. USUI, AND C. PARIMI, *Arbitrary discontinuities in finite elements*, Internat. J. Numer. Methods Engrg., 50 (2001), pp. 993–1013.
[5] S. BERRONE, S. PIERACCINI, AND S. SCIALÒ, *On simulations of discrete fracture network flows with an optimization-based extended finite element method*, SIAM J. Sci. Comput., 35 (2013), pp. A908–A935.
[6] M. C. CACAS, E. LEDOUX, G. DE MARSILY, B. TILLIE, A. BARBREAU, E. DURAND, B. FEUGA, AND P. PEAUDECERF, *Modeling fracture flow with a stochastic discrete fracture network: Calibration and validation: 1. The flow model*, Water Resource Res., 26 (1990), pp. 479–489.
[7] J. CHESSA, H. WANG, AND T. BELYTSCHKO, *On the construction of blending elements for local partition of unity enriched finite elements*, Internat. J. Numer. Methods Engrg., 57 (2003), pp. 1015–1038.
[8] C. DAUX, N. MÖES, J. DOLBOW, N. SUKUMAR, AND T. BELYTSCHKO, *Arbitrary branched and intersecting cracks with the extended finite element method*, Internat. J. Numer. Methods Engrg., 48 (2000), pp. 1741–1760.

[9] W. S. Dershowitz and H. H. Einstein, *Characterizing rock joint geometry with joint system models*, Rock Mechanics and Rock Engineering, 1 (1988), pp. 21–51.

[10] W. S. Dershowitz and C. Fidelibus, *Derivation of equivalent pipe networks analogues for three-dimensional discrete fracture networks by the boundary element method*, Water Resource Res., 35 (1999), pp. 2685–2691.

[11] J. Erhel, J.-R. de Dreuzy, and B. Poirriez, *Flow simulation in three-dimensional discrete fracture networks*, SIAM J. Sci. Comput., 31 (2009), pp. 2688–2705.

[12] C. Fidelibus, *The 2D hydro-mechanically coupled response of a rock mass with fractures via a mixed BEM-FEM technique*, Internat. J. Numer. Anal. Methods in Geomechanics, 31 (2007), pp. 1329–1348.

[13] T.-P. Fries, *A corrected XFEM approximation without problems in blending elements*, Internat. J. Numer. Methods Engrg., 75 (2008), pp. 503–532.

[14] T.-P. Fries and T. Belytschko, *The extended/generalized finite element method: An overview of the method and its applications*, Internat. J. Numer. Methods Engrg., 84 (2010), pp. 253–304.

[15] V. Girault and R. Glowinski, *Error analysis of a fictitious domain method applied to a Dirichlet problem*, Japan J. Indust. Appl. Math., 12 (1995), pp. 487–514.

[16] R. A. Horn and C. A. Johnson, *Matrix Analysis*, Cambridge University Press, Cambridge, UK, 1985.

[17] T. Kalbacher, R. Mettier, C. McDermott, W. Wang, G. Kosakowski, T. Taniguchi, and O. Kolditz, *Geometric modelling and object-oriented software concepts applied to a heterogeneous fractured network from the grimsel rock laboratory*, Comput. Geosci., 11 (2007), pp. 9–26.

[18] J. L. Lions, *Optimal Control of Systems Governed by Partial Differential Equations*, Grundelhren Math. Wisse. 170, Springer-Verlag, Berlin, 1971.

[19] I. Miller, G. Lee, and W. Dershowitz, *MAFIC Matrix/Fracture Interaction Code With Heat and Solute Transport User Documentation, Version* 1.6, Golder Associates, Redmond, WA, 1997.

[20] H. Mustapha and K. Mustapha, *A new approach to simulating flow in discrete fracture networks with an optimized mesh*, SIAM J. Sci. Comput., 29 (2007), pp. 1439–1459.

[21] J. Nocedal and S. Wright, *Numerical Optimization*, Springer, Berlin, 1999.

[22] A. W. Nordqvist, Y. W. Tsang, C. F. Tsang, B. Dverstop, and J. Andersson, *A variable aperture fracture network model for flow and transport in fractured rocks*, Water Resource Res., 28 (1992), pp. 1703–1713.

[23] G. Pichot, J. Erhel, and J.-R. De Dreuzy, *A mixed hybrid Mortar method for solving flow in discrete fracture networks*, Appl. Anal., 89 (2010), pp. 1629–1643.

[24] G. Pichot, J. Erhel, and J.-R. de Dreuzy, *A generalized mixed hybrid mortar method for solving flow in stochastic discrete fracture networks*, SIAM J. Sci. Comput., 34 (2012), pp. B86–B105.

[25] T. Strouboulis, I. Babuška, and K. Copps, *The design and analysis of the generalized finite element method*, Comput. Methods Appl. Mech. Engrg., 181 (2000), pp. 43–69.

[26] T. Strouboulis, K. Copps, and I. Babuška, *The generalized finite element method: An example of its implementation and illustration of its performance*, Internat. J. Numer. Methods Engrg., 47 (2000), pp. 1401–1417.

[27] N. Sukumar, D. Chopp, N. Möes, and T. Belytschko, *Modeling holes and inclusions by level sets in the extended finite element method*, Comput. Methods Appl. Mech. Engrg., 190 (2001), pp. 1209–1233.

[28] M. Vohralík, J. Maryška, and O. Severýn, *Mixed and nonconforming finite element methods on a system of polygons*, Appl. Numer. Math., 51 (2007), pp. 176–193.

[29] L. B. Wahlbin, *Local Behavior in Finite Element Methods*, vol. 2, Handb. Numer. Anal., North-Holland, Amsterdam, 1991, pp. 353–522.